Cold collisions between atoms and diatomic molecules

M. Lysebo* and L. Veseth
Department of Physics, University of Oslo, 0316 Oslo, Norway
(Received 11 October 2007; published 24 March 2008)

Collision cross sections are calculated for the three systems O_2-He, Na_2-Na and K_2-K at cold and ultracold temperatures. We discuss their relevance for cold molecule formation by buffer-gas cooling and by other cooling methods where collisions between molecules and atoms are important, e.g photoassociation. The molecule is treated as a rigid rotator in the electronic and vibrational ground state. We have calculated *ab initio* the potential energy surfaces for the three systems with special emphasis on the long range potential which is very important at low energies. With relevance to buffer gas cooling, we have also studied the thermalization process between O_2 molecules and He atoms as determined by the calculated cross sections.

DOI: 10.1103/PhysRevA.77.032721 PACS number(s): 34.20.−b, 31.50.Bc, 34.50.−s

I. INTRODUCTION

Ultracold molecules are now regularly produced in many laboratories around the world. The cooling of molecules requires some rather sophisticated techniques, due to the fact that molecules cannot be cooled to very low temperatures by the methods applicable to atoms, e.g., laser cooling. Laser cooling is efficient only for two-level systems, whereas molecules are in general multilevel systems [1].

New methods are therefore needed to produce ultracold molecules. One approach that works in particular for the alkalis is to start from samples of ultracold atoms. With samples of ultracold atoms available several procedures have in fact been able to produce even molecular Bose-Einstein condensates, which were first observed in 2003 [2–4].

Feshbach resonances [5] have proved to be a valuable tool in ultracold atomic physics, indeed, also in ultracold molecule formation. In fact the first molecular Bose-Einstein condensates were created from ultracold atoms, converted to molecules by utilizing Feshbach resonances. Unfortunately molecules formed from Feshbach resonances will generally have short lifetimes, and they will normally be formed in highly excited vibrational levels, i.e., be vibrationally very hot.

Different one- or two-color photoassociation [6,7] procedures have also been widely used to create molecules in the ultracold (<1 μK) temperature range. Molecules formed by use of photoassociation techniques will also generally end up in high vibrational states, but the end products will in this case depend very much on the atomic species and the detailed photoassociation scheme. In addition, use of the above mentioned methods requires detailed spectroscopic information that may not be available in an accurate manner.

A different and very general cooling method is buffer-gas cooling, first proposed by Stwalley [8]. The method is applicable to atoms as well as molecules. Buffer-gas cooling requires no knowledge of spectroscopic details; the only requirement is of course that reactive collisions with the buffer gas are avoided. Any inert gas may be used as a buffer gas, although ^{3}He is preferred due to its high vapor pressure at low temperatures. The initially hot molecules disperse their energy onto the buffer-gas atoms and are rethermalized. Unfortunately, buffer-gas cooling does not lead to temperatures that are low enough to enable Bose-Einstein condensates. However, by combining buffer-gas cooling with magnetic trapping [9], molecules may be evaporatively cooled to ultracold temperatures.

For buffer-gas cooling and subsequent evaporative cooling to be effective, it is of paramount importance that the relevant cross sections are favorable. Buffer-gas cooling will be most effective when elastic cross sections are large. Inelastic collisions (state changing collisions) are often referred to as bad collisions in this context. This is not necessarily true, e.g., collisions where the rotational quantum number is reduced will help to cool the rotational degree of freedom. However, inelastic collisions are often associated with trap loss. Collisions that change the Zeeman level from high-field seeking to low-field seeking will certainly cause trap loss for magnetic trapping.

In the present work we have investigated a particular type of cold collisions, namely cold spin-changing collisions between nonpolar diatomic molecules and atoms. Throughout this paper we assume that the molecules are in their ground electronic state and also in their lowest vibrational level ($v=0$).

Collisions involving molecules represent an extra challenge, as the atom-molecule interaction is certainly more complex than that for atom-atom collisions. In addition, even for cold collisions molecules will have a large variety of available final states (open channels).

Whereas interatomic potentials are often known or can be readily calculated with high accuracy, potential energy surfaces (PES) related to molecular interactions are harder to obtain and might be less accurate. However, the low temperature allows for simplifications. It will, for instance, generally be sufficient to treat the molecule as a rigid rotator with the internuclear separation fixed at the equilibrium distance.

Both atomic- and molecular cross sections are known to be very sensitive to the long-range potential. Often the long-range potential is simply written as $V(r)=-C_6/r^6$ with C_6 determined from fitting $V(r)$ to the long range part of the calculated PES. In this study we adopt a different approach and calculate what we believe to be very accurate long-range

*marius.lysebo@fys.uio.no

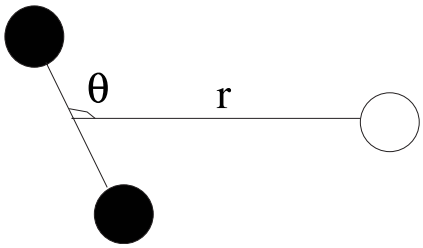

FIG. 1. Definition of r and θ. The diatomic molecule is indicated by the solid circles.

potentials based on the atomic and molecular polarizabilities

Studies similar to the present one on cold atom–diatomic molecule collisions have been presented in several other recent works. Bohn [10] has previously calculated selected cross sections for the O_2-He interaction with different O_2 isotopes [10]. Ultracold collisions between $Na_2[^3\Sigma_u^+(v=1)]$ and Na have also been studied [11], as well as collisions involving the same electronic and vibrational states for the systems Li_2-Li [12] and K_2-K [13].

II. SCATTERING CALCULATIONS

A. Obtaining the *S* matrix

Computation of cross sections require solving a large set of coupled differential equations. The method used to solve these equations in the present study has been described elsewhere by several authors [10,14,15]. Here we only provide an overview of the method, starting with the Hamiltonian for the whole system (molecule+atom)

$$H = -\frac{\hbar^2}{2\mu}\nabla^2 + H_{\text{int}} + V(r,\theta). \tag{1}$$

r and θ are defined according to Fig. 1 and H_{int} is the internal Hamiltonian for both systems including the molecular fine structure. The total wave function with internal quantum numbers collectively labeled p, and orbital angular momentum L with projection M may be written

$$\Psi_{pLM} = \frac{1}{r}\psi^{\mathcal{J}}_{pLM}(r)\psi_p(\mathbf{r}_1)Y_{LM}(\theta',\phi'), \tag{2}$$

with $\psi_p(\mathbf{r}_1)$ as eigenstates of H_{int}. θ',ϕ' is the orientation of a vector from the molecular center of mass to the atom referred to in the laboratory system. The N coupled differential equations are obtained from the Schrödinger equation and may be written [15]

$$\left[\frac{d^2}{dr^2} + k_p^2 - \frac{L(L+1)}{r^2}\right]\psi^{\mathcal{J}}_p(r) = \sum_{p'}\langle pL;\mathcal{J}|\frac{2\mu}{\hbar^2}V(r,\theta)|p'L';\mathcal{J}\rangle\psi^{\mathcal{J}}_{p'}. \tag{3}$$

In Eq. (3) p and p' are internal states for both molecule and atom and $\psi^{\mathcal{J}}_p(r)$ is the radial wave function for total angular momentum $\mathcal{J}$. k_p is defined as

$$k_p^2 \equiv \frac{2\mu}{\hbar^2}(E - E_p), \tag{4}$$

with μ as the reduced mass and E_p as the asymptotic energy in a channel with internal quantum numbers p. The number of channels involved in a calculation can be large. All relevant internal molecular states must be included, along with an adequate number of partial waves to ensure convergence for the given energy. Although we include many channels it is important to remember that we do not allow for reactive scattering; thus the molecular bonds cannot be broken during a collision. Reactive scattering should be very limited at most of the temperatures we investigate.

The total angular momentum quantum number $\mathcal{J}$ is defined as

$$\mathcal{J} = \mathbf{N} + \mathbf{S} + \mathbf{s} + \mathbf{L}, \tag{5}$$

where we have assumed that the atom is without angular momentum (s state). $\mathbf{N}$ is the molecular angular momentum, $\mathbf{S}$ is the molecular spin, whereas $\mathbf{s}$ is the atomic spin. $\mathbf{L}$ is the partial wave angular momentum representing rotation of molecule+atom about their center of mass. We also introduce $\mathbf{J}_m = \mathbf{N}+\mathbf{S}$ as the total molecular angular momentum, and $\mathbf{J}_1 = \mathbf{s}+\mathbf{L}$.

For a given collision, without a magnetic field, the total angular momentum $\mathcal{J}$ is conserved. However, we do allow $\mathbf{N}$ and $\mathbf{L}$ (and thereby $\mathbf{J}_m$ and $\mathbf{J}_1$) to change in a collision.

To calculate the matrix elements $\langle pL;\mathcal{J}|U|p'L';\mathcal{J}\rangle$ the first step is to express the anisotropic potential $V(r,\theta)$ in terms of Legendre polynomials $P_l(\cos\theta)$

$$V(r,\theta) = \sum_l v_l(r)P_l[\cos(\theta)]. \tag{6}$$

Generally the number of Legendre polynomials included in the sum in Eq. (6) will be large when the potential is strongly anisotropic. With Eq. (6) we may write

$$\langle pL;\mathcal{J}|U|p'L';\mathcal{J}\rangle = \frac{2\mu}{\hbar^2}\sum_l v_l(r)\langle pL;\mathcal{J}|P_l(\cos\theta)|p'L';\mathcal{J}\rangle. \tag{7}$$

Equation (7) may be further simplified by use of the addition theorem for renormalized spherical harmonics

$$P_l(\cos\theta) = \mathbf{C}_l(\mathbf{R})\cdot\mathbf{C}_l(\mathbf{R}'). \tag{8}$$

In Eq. (8) $\mathbf{R}=(\theta_m,\phi_m)$ is the direction of the molecular axis referred to the laboratory system. With this definition we have $\theta=\theta_m-\theta'$.

Next we use the Wigner-Eckart theorem to obtain

$$\langle pL;\mathcal{J}|P_l(\cos\theta)|p'L';\mathcal{J}\rangle = [J_m][J_1][N][L][J'_m][J'_1][N'][L'] \times(-1)^{\mathcal{J}-S-s+3J_2+J'_2+2J_1+2J'_1+N+N'+L+L'} \begin{Bmatrix} J_m & J'_m & l \\ J'_1 & J_1 & \mathcal{J} \end{Bmatrix} \times \begin{Bmatrix} N & N' & l \\ J'_m & J_m & S \end{Bmatrix} \begin{Bmatrix} L & L' & l \\ J'_1 & J_1 & s \end{Bmatrix} \begin{pmatrix} l & N' & N \\ 0 & 0 & 0 \end{pmatrix} \begin{pmatrix} l & L' & L \\ 0 & 0 & 0 \end{pmatrix}. \quad (9)$$

To ease the notation we have defined $[J_m] \equiv \sqrt{(2J_m+1)}$ and so on. Upon deriving Eq. (9) we have used Eqs. (4.17) and (5.13) of [16]. In Eq. (9) {…} denotes 6*j* symbols and (…) are 3*j* symbols.

To define the scattering matrix we construct a superposition of the wave functions $\psi_p(\mathbf{r})$ which in general defines the electronic, vibrational, and rotational states of the two colliding systems. Before and after a collision the whole system must be represented by the superposition

$$\Psi(\mathbf{r}_1) = \sum_p a_p \psi_p(\mathbf{r}_1), \quad (10)$$

where $|a_p|^2$ represents the probability of finding the system in eigenstate $\psi_p(\mathbf{r}_1)$. Clearly the coefficients *a* define the state completely for a finite set of quantum numbers *p*. We use the vector $A=[a_{p_1}, a_{p_2}, \ldots, a_{p_n}]^T$ to formally define the scattering matrix by the equation

$$A_f = SA_i. \quad (11)$$

A_i and A_f are the asymptotic states of the system before and after the collision, respectively. This important scattering matrix (*S* matrix) is obtained numerically with the log derivative method first introduced by Johnsen [17]. We have implemented this algorithm and used a local cluster of 30 1.00 GHz Linux PCs to do the actual calculations; this was achieved with a trivial parallelization where each machine gets assigned a specific energy.

B. Calculation of cross sections

The vast majority of the total CPU time needed for scattering calculations is spent solving the coupled differential equations to obtain the *S* matrix. Once the *S* matrix is found, the state to state cross sections can be calculated as a sum over the relevant *S*-matrix elements.

The asymptotic solution ψ_{pLM} outside the range of the potential $V(r,\theta)$ has to satisfy the equation

$$-\frac{\hbar^2}{2\mu}\left\{\frac{d^2}{dr^2} - \frac{L(L+1)}{r^2}\right\}\psi^{\mathcal{J}}_{pLM}(r) = (E-E_p)\psi^{\mathcal{J}}_{pLM}(r). \quad (12)$$

Thus $\psi^{\mathcal{J}}_{pLM}(r)$ can be written

$$\psi^{\mathcal{J}}_{pLM}(r) = \frac{1}{k_p}(A_{pLM}e^{-i(k_p r - L\pi/2)} + B_{pLM}e^{i(k_p r - L\pi/2)}). \quad (13)$$

The relevant coefficients A_{pLM} and B_{pLM} are found out of a comparison with the total wave function for a plane incoming wave with wave vector $\mathbf{k}_p$ in the direction given by (θ_k, ϕ_k)

$$e^{i\mathbf{k}_p\cdot\mathbf{R}'}\psi_p = \frac{2\pi}{k_p r}\sum_{LM}\{i^L Y^*_{LM}(\theta_k,\phi_k) \times(e^{i(k_p r - L\pi/2} - e^{-i(k_p r - L\pi/2)})Y_{LM}(\theta',\phi')\}\psi_p. \quad (14)$$

It is found that $A_{pLM} = -B_{pLM} = -(2\pi/ik_p)i^L Y^*_{LM}(\theta_k,\phi_k)$. From the definition of the *S*-matrix elements we may write $B_{p'L'M'} = S^{p'L'M'}_{pLM}A_{pLM}$. We use this to construct a total wave function with an incoming plane wave in internal state *p* and an outgoing spherical wave in a superposition of different internal states *p'*

$$\Psi_p = \frac{2\pi}{irk_p^{1/2}}\left(\sum_{LM} i^L Y^*_{LM}(\theta_k,\phi_k)k_p^{-1/2}e^{-i(k_p r - L\pi/2)}Y_{LM}(\theta',\phi')\psi_p + \sum_{p'L'M'} i^{L'}Y^*_{LM}(\theta_k,\phi_k)k_{p'}^{-1/2}S^{p'L'M'}_{pLM} \times e^{i(k_{p'}r - L'\pi/2)}Y_{L'M'}(\theta',\phi')\psi_{p'}\right). \quad (15)$$

By comparison with the well known total wave function for large *r*

$$\Psi_p = \psi_p e^{i\mathbf{k}_p\cdot\mathbf{r}} + \sum_{p'} f_{p'}\frac{e^{ik_{p'}r}}{r}\psi_{p'}, \quad (16)$$

it is possible to identify the scattering amplitude $f_{p'}(\theta',\phi')$ for scattering in direction (θ',ϕ'),

$$f_{p'}(\theta',\phi') = \frac{2\pi}{i(k_p k_{p'})^{1/2}}\sum_{LM} i^L Y^*_{LM}(\theta_k,\phi_k)\sum_{L'M'} e^{-iL\pi/2} \times[S^{p'L'M'}_{pLM} - \delta_{pp'}\delta_{LL'}\delta_{MM'}]Y_{L'M'}(\theta',\phi'). \quad (17)$$

Closely related to the scattering amplitude is the differential cross section, which may be calculated from the connection $d\sigma/d\Omega = (k_{p'}/k_p)|f_{p'}|^2$. In addition, we average over the incident directions (θ_k,ϕ_k) to find that the cross section is given by the equation

$$\sigma_{p\to p'} = \frac{\pi}{k_p^2}\sum_{LML'M'}|S^{p'L'M'}_{pLM} - \delta_{pp'}\delta_{LL'}\delta_{MM'}|^2. \quad (18)$$

III. POTENTIAL ENERGY SURFACES

A. Short range potential

We have investigated the three systems O_2-He, Na_2-Na, and K_2-K. For all systems we have needed to calculate potential energy surfaces (PES). For small internuclear separations ($r<20$ a.u.) we have used the quantum chemistry package GAMESS [18]. In these calculations we started with a UHF self-consistent field molecular wave functions for all the systems. In particular, for the O_2-He complex we need

TABLE I. Basis sets used with GAMESS to calculate the different short range potential energy surfaces. Similar types of Dunning's correlation consistent basis sets are used for O_2-He and Na_2-Na, whereas the TZV (triple valence) basis set is used for K_2-K.

System	Basis set used for atoms in the molecule	Basis set for the lone atom	Basis ref.
O_2-He	aug-cc-pCVTZ	aug-cc-pCVTZ	[21–23]
Na_2-Na	cc-pVTZ	cc-pVTZ	[23]
Ka_2-Ka	TZV	TZV	[24]

the UHF wave function due to the Hartee-Fock instability of O_2 as reported previously by van Lenthe and van Duijneveldt [19]. The Hartree-Fock wave function is used as a starting point for a more accurate treatment based on the Møller-Plesset perturbation theory.

We have calculated second order energy corrections with MP2 [20]. The basis sets used are reported in Table I [21–24].

No frozen core orbitals have been kept in our MP2 calculations. To obtain the internuclear interactions we have used the supermolecular approach [25]. This implies that for all geometries three calculations are needed. First we calculate the MP2 energy for the total system consisting of atom +molecule; thereafter, we perform calculations with the molecule together with a ghost atom.

A ghost atom does not have a positively charged nucleus but the atomic orbitals are kept. Here we use the counterpoise correction method [26] with ghost atoms to reduce the basis set superposition error. For each geometry this involves also a calculation of the MP2 energy with the atom and the ghost molecule. Finally, to obtain the PES, the energies of the two calculations involving ghost basis sets are added and the result is subtracted from the energy of the whole complex. Generally for two atoms or molecules A and B at geometry $\mathbf{G}$ we calculate

$$V_{AB}(\mathbf{G}) = E_{AB}(\mathbf{G}) - E_A(\mathbf{G}) - E_B(\mathbf{G}), \tag{19}$$

with E_{AB} as the energy obtained for both systems A and B, whereas E_A and E_B are the respective energies obtained with only system A or system B. For all calculations the basis sets are the same as for the full calculation AB.

B. Long range potentials

At long distances the interaction potential between an atom and a nonpolar diatomic molecule takes the approximate form (cf. Fig. 1):

$$V(r,\theta) = -\frac{1}{r^6}[C_6^{(0)} + C_6^{(2)}P_2(\cos\,\theta)] - \frac{1}{r^8}[C_8^{(0)} + C_8^{(2)}P_2(\cos\,\theta) + C_8^{(4)}P_4(\cos\,\theta)]. \tag{20}$$

The dispersion coefficients (Van der Waals coefficients) $C_6^{(0)}$, $C_6^{(2)}$, $C_8^{(0)}$, $C_8^{(2)}$, and $C_8^{(4)}$ may be expressed in terms of the polarizabilities of the atom and the molecule. The lowest-order coefficients $C_6^{(0)}$ and $C_6^{(2)}$ are determined by the dipole polarizabilities, whereas quadrupole and octupole polarizabilities are needed to determine the coefficients $C_8^{(0)}$, $C_8^{(2)}$, and $C_8^{(4)}$.

The frequency dependent (dynamic) dipole polarizability for an atom is given by the expression

$$\alpha_1^A(\omega) = -\sum_{k(\neq n)} \frac{|\langle\psi_k|\sum_{i=1}^N z_i|\psi_n\rangle|^2}{E_n - E_k \pm \omega}, \tag{21}$$

where E_k and $|\psi_k\rangle$ respectively denote eigenvalues and eigenstates of the atomic system with N electrons. The double sign in the denominator indicates a sum of two terms, one with + and the other with −. For a diatomic molecule one has to consider the polarizability $\alpha_\parallel(\omega)=\alpha_{zz}$ along the molecular axis and the polarizability $\alpha_\perp(\omega)=\alpha_{xx}(\omega)=\alpha_{yy}(\omega)$ perpendicular to the axis. The expression for $\alpha_\parallel(\omega)$ is identical to that of Eq. (21), whereas $\alpha_\perp(\omega)$ is obtained from Eq. (21) by replacing z_i with x_i or y_i. Finally, the polarizabilities that will be needed for a diatomic molecule are the average polarizability

$$\bar{\alpha}(\omega) = \frac{1}{3}[2\alpha_\perp(\omega) + \alpha_\parallel(\omega)] \tag{22}$$

and the anisotropy

$$\Delta\alpha(\omega) = \alpha_\parallel(\omega) - \alpha_\perp(\omega). \tag{23}$$

Unfortunately, Eq. (21) is not very useful to compute dynamic polarizabilities, as singular frequencies will be encountered at the excited energies E_k. However, it turns out that the dispersion coefficients are actually determined by the polarizabilities at imaginary frequencies $i\eta$. At imaginary frequencies there are no singularities and the polarizabilities are real positive numbers that decrease monotonically from their maximum at $\eta=0$. Similar properties are also found for the quadrupole and octupole polarizabilities at imaginary frequencies.

A method for accurate computation of dynamic polarizabilities at imaginary frequencies has been presented in a previous work by one of the present authors [27]. Diagrammatic many-body theory is used, with complete inclusion of all diagrams representing up to two interactions with the electronic repulsion term $1/r_{12}$. This means a substantial inclusion of electron correlation and, with reference to Eq. (21), that the polarizabilities are expected to be computed with very accurate eigenvalues and eigenstates. The same technique also applies to the quadrupole and octupole polarizabilities; the dipole components merely have to be replaced by the relevant quadrupole or octupole moments.

The expressions for the dispersion coefficients $C_6^{(0)}$ and $C_6^{(2)}$ are fairly simple [28,29]:

$$C_6^{(0)} = \frac{3\hbar}{\pi}\int_0^\infty \alpha_1^A(i\eta)\bar{\alpha}(i\eta)d\eta, \tag{24}$$

TABLE II. Computed dipole polarizabilities (a.u.) at the imaginary frequencies $i\eta$(a.u.) for the electronic ground states of O_2 and Na_2. The computed values are at the respective equilibrium internuclear distances.

	O_2		Na_2	
η	$\alpha_\parallel$	$\alpha_\perp$	$\alpha_\parallel$	$\alpha_\perp$
0.00	14.68	5.73	347.2	184.3
0.10	13.84	5.60	164.0	109.5
0.20	12.28	5.28	45.5	42.3
0.30	10.63	4.88	15.9	18.5
0.40	9.09	4.45	7.17	9.76
0.50	7.74	4.03	3.81	5.95

$$C_6^{(2)} = \frac{\hbar}{\pi}\int_0^\infty \alpha_1^A(i\eta)\Delta\alpha(i\eta)d\eta. \tag{25}$$

The expressions for the higher-order dispersion coefficients $C_8^{(0)}$, $C_8^{(2)}$, and $C_8^{(4)}$ are rather complex and are not reproduced here. Complete expressions can be found in the papers by Bishop and Pipin [28] and Hohm [29], and references therein. Table II gives computed dipole polarizabilities at some selected imaginary frequencies for the diatomic molecules O_2 and Na_2. The computed dispersion coefficients are shown in Table III. The results presented are for the systems He-O_2, Na-Na_2, and K-K_2, which are the systems of current interest.

IV. O_2-He SYSTEM

In the present work we consider the ^{3}He isotope and calculate cross sections for collisions with $^{16}O_2$ molecules. The O_2 molecule is treated as a rigid rotator with an internuclear separation of r_e=1.2165 Å. We discuss how the calculated cross sections are relevant for both buffer-gas cooling of O_2 molecules as well as for magnetic trapping of O_2 molecules with He atoms present.

The ground state of the O_2 molecule has the designation $^3\Sigma_g^-$. The rotational structure together with the **J**=**N**+**S** fine structure are shown in Fig. 2 for the ground electronic and vibrational state [30]. Note that even rotational levels are not allowed in the ground state due to the Pauli principle which requires the total molecular wave function to be symmetric whenever the nuclear spin is equal to zero [31].

The calculated, short range PES is reported in Table IV. From Table IV and the PES it is readily seen that the He atom is most strongly repelled from the O_2 molecule when approaching at an angle θ=0°. Least repulsion is experienced for θ=90°, where the PES is also deepest with a maximum depth of 110μE_h for r=5.95 a.u.

TABLE III. Computed dispersion coefficients (a.u.) [cf. Eq. (20)].

	$C_6^{(0)}$	$C_6^{(2)}$	$C_8^{(0)}$	$C_8^{(2)}$	$C_8^{(4)}$
He-O_2	7.05	1.67	142.2	134.2	70.0
Na-Na_2	2701.8	512.8	328170	157820	129350
K-K_2	4786.1	1540.4	518920	394400	260420

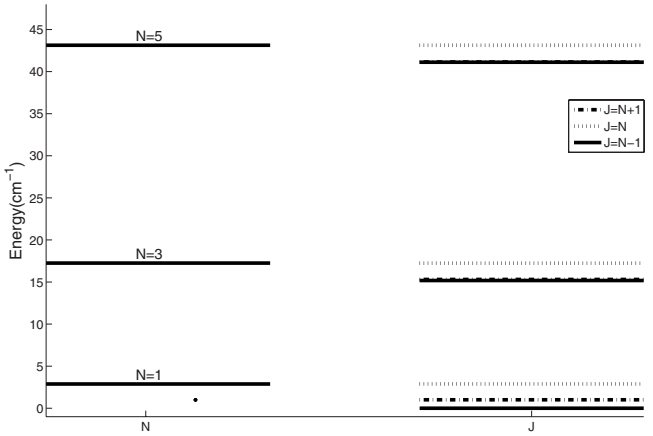

FIG. 2. Rotational structure for the O_2 electronic ground state, v=0. Values for the fine structure are from [30]. The energy difference between some of the levels are too small to be fully resolved in the figure.

The PES is expanded in Legendre polynomials; cf. Eq. (6). The functions $v_l(r)$ are easily found by using the orthogonality relation for the Legendre polynomials and by performing the relevant integrals numerically. The functions $v_0(r)$–$v_{10}(r)$ are shown in Fig. 3.

Figure 3 reveals that the isotropic term $v_0(r)$ dominates over the anisotropic terms. The PES is in fact quite isotropic which can also be seen from Table IV; the anisotropic effects present in the PES are largely carried by the terms $v_2(r)$ and $v_4(r)$. The long range part of the potential becomes more important as the temperature decreases, and for ultracold temperatures it is necessary to integrate the coupled equations [Eq. (3)] to large values of r. We have integrated from r=5 a.u. out to r=2000 a.u. to ensure proper convergence of the cross sections. For temperatures around 1 μK, only the L=0 partial wave (s wave) contributes. To obtain a satisfactory convergence of the cross sections we include an increasing number of partial waves with increasing temperature. For the highest calculated temperature, 20 K, we include all partial waves L=0–35 to achieve sufficient convergence of the cross sections. Both closed and open channels were included, this meaning that the total number of channels involved exceeds 1000.

A. Cross sections

Here we report both elastic and inelastic cross sections for O_2-He collisions. We consider O_2 molecules in the N=1 rotational level as well as the excited N=3 level. The state to state cross sections we present may be relevant for magnetic trapping, thus we have included the different Zeeman levels M_j. See [15] or [10] for details on how to convert the S-matrix to the appropriate basis in which cross sections involving magnetic quantum numbers can be computed. Cross sections for N=1 at temperatures T=10^{-6}–10 K are shown in Fig. 4.

TABLE IV. Calculated PES for O_2-He. Distances r in a.u. and angles θ in degrees. Energies in μE_h. We have used the basis set aug-cc-pCVTZ [21–23] for both the O_2 atom and the He atom. All values obtained with the quantum chemistry package GAMESS [18].

	θ									
r	0	10	20	30	40	50	60	70	80	90
5.00	5496	5324	4854	4148	3266	2327	1401	839.1	450.7	321.2
5.50	1466	1429	1314	1123	867.6	585.9	326.6	127.1	5.878	−34.53
6.00	271.8	267.8	250.3	212.7	151.7	76.55	3.967	−53.53	−89.34	−107.4
6.50	−40.28	−37.42	−24.72	−21.21	−22.77	−36.94	−58.10	−77.89	−91.42	−95.99
7.00	−94.86	−92.18	−85.14	−76.74	−70.79	−68.53	−68.84	−69.92	−71.26	−71.19
8.00	−60.75	−59.48	−56.15	−51.85	−47.28	−43.03	−39.45	−36.74	−35.12	−34.59
9.00	−29.65	−29.26	−27.83	−26.07	−23.85	−21.73	−19.85	−18.26	−17.12	−17.02
10.0	−14.88	−14.65	−14.08	−13.27	−12.26	−11.23	−10.30	−9.525	−9.045	−8.892
11.0	−7.956	−8.020	−7.584	−7.165	−6.665	−6.142	−5.655	−5.270	−5.119	−4.939
12.0	−4.532	−4.515	−4.278	−4.106	−2.330	−3.548	−3.945	−3.076	−2.969	−2.894
14.0	−1.704	−1.674	−1.548	−1.548	−1.847	−1.362	−1.278	−1.190	−1.030	−1.128
16.0	−0.7425	−0.7145	−0.6808	−0.6437	−0.6281	−0.5951	−0.5558	−0.5280	0.5000	−0.5011

The cross sections are calculated at zero magnetic field. From a computational point of view, zero magnetic field is convenient as the different $\mathcal{J}$ values do not interact and may be computed separately. The cross sections will of course be somewhat modified by the presence of a magnetic field, in particular the energies at which different resonances occur. The resonance seen in Fig. 4 at $T \simeq 0.9$ K will most certainly reassert itself at a different energy in a magnetic field, although we expect the general behavior of the cross sections to be similar. Even though a magnetic field may alter the cross sections, we comment below on their relevance for magnetic trapping. At the center of a magnetic trap, the magnetic field will be small or simply vanish. Thus the perturbation on the system caused by the magnetic field should yield only small changes in the overall behavior of the cross sections, in particular for geometries close to the center of the trap.

It is evident from Fig. 4 that the inelastic cross sections are several orders of magnitudes smaller than the elastic cross sections. This is certainly encouraging for experiments that involve buffer-gas cooling of magnetically trapped O_2 molecules. In particular for low temperatures elastic scattering is seen to be by far dominating (in the lowest rotational level), thus minimizing the number of collisions between O_2 molecules and He atoms that lead to trap loss. One also needs to be aware that inelastic scattering does not necessar-

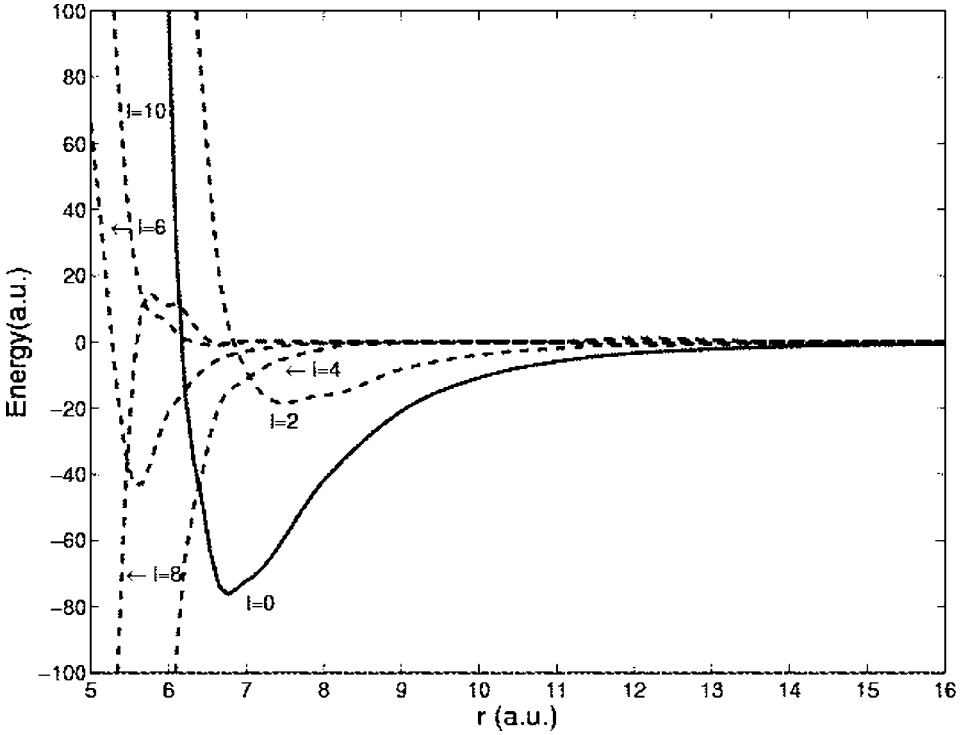

FIG. 3. $v_l(r)$ for $l=0,2,4,6,8,10$. $v_l(r)$ is zero for odd l since the PES is symmetric about $\theta=90°$. The isotropic contribution is plotted as a solid line.

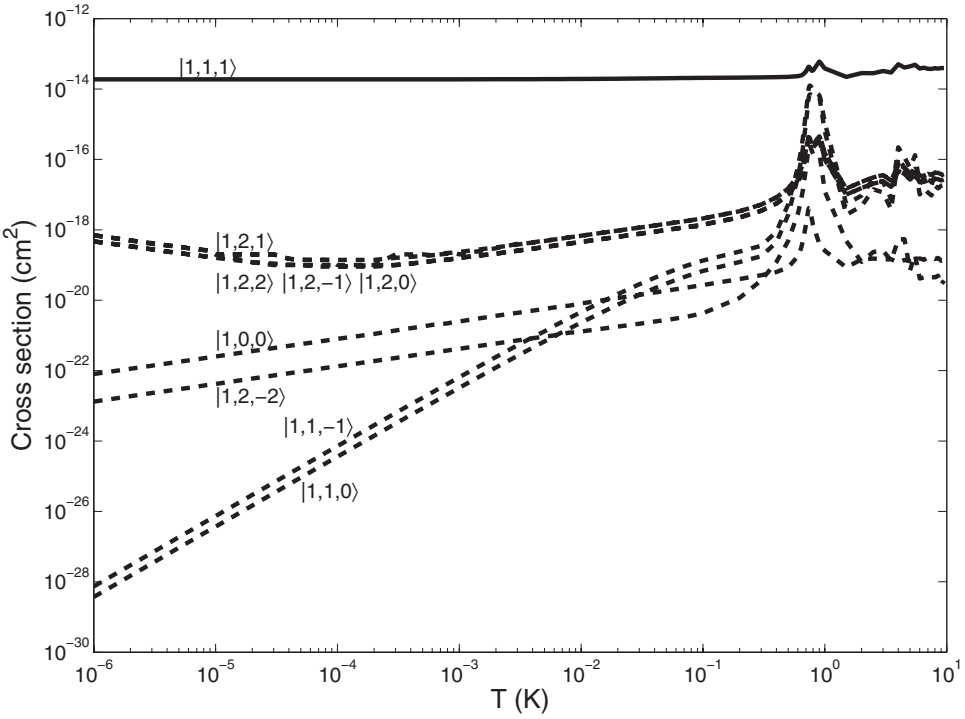

FIG. 4. Cross sections for both elastic (solid line) and inelastic scattering (dashed lines) $|N,J,M_J\rangle \rightarrow |N',J',M_J'\rangle$ for $N=1, J=1, M_J=1$. Away from any resonances the elastic scattering process is seen to be dominating in the $N=1$ rotational level.

ily result in trap loss as the final channel may involve M_J quantum numbers larger than zero, making the final state magnetically trapable. In Fig. 5 we give the partial waves $L=0,1,2$ for the elastic scattering process $|N=1,J=1,M_J=1\rangle \rightarrow |1,1,1\rangle$. The Wigner threshold law [32] (for elastic scattering)

$$\sigma_{\mathrm{el}} \propto E^{2L} \tag{26}$$

can be seen to be obeyed in Fig. 5 for temperatures $T < 10^{-3}$ K. From Fig. 5 it is also evident that partial waves $L>0$ give only a negligible contribution to the total cross section for temperatures in the mK range.

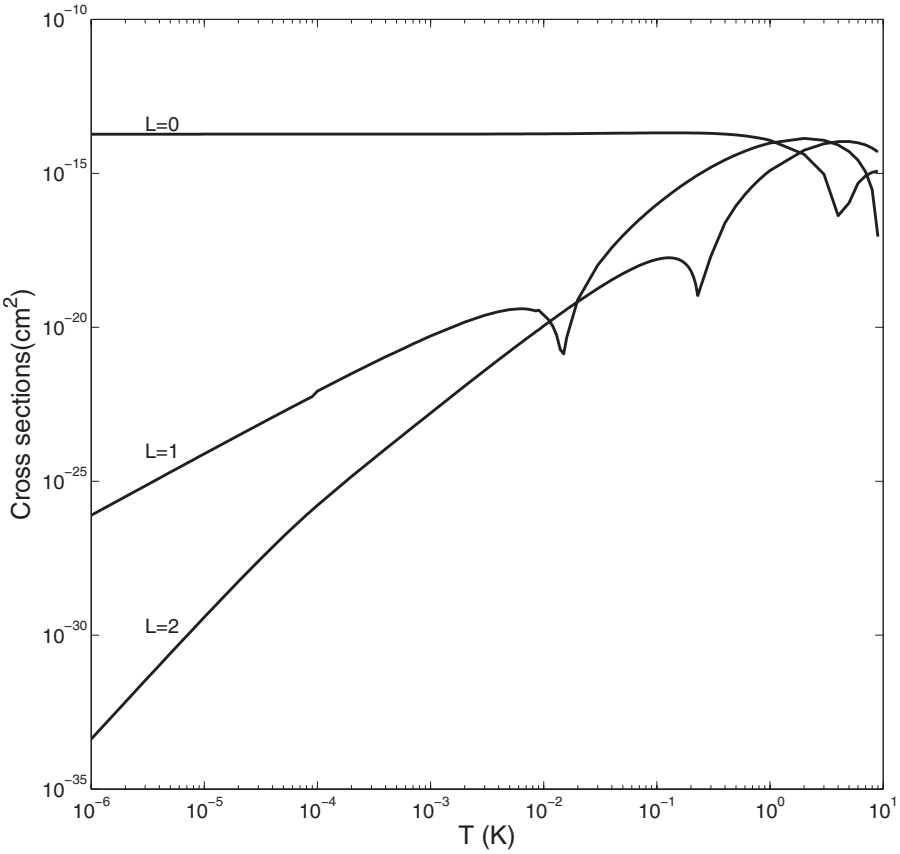

FIG. 5. Contributions to elastic cross sections from partial waves $L=0,1,2$ as a function of temperature. The partial wave cross sections follow the Wigner threshold law.

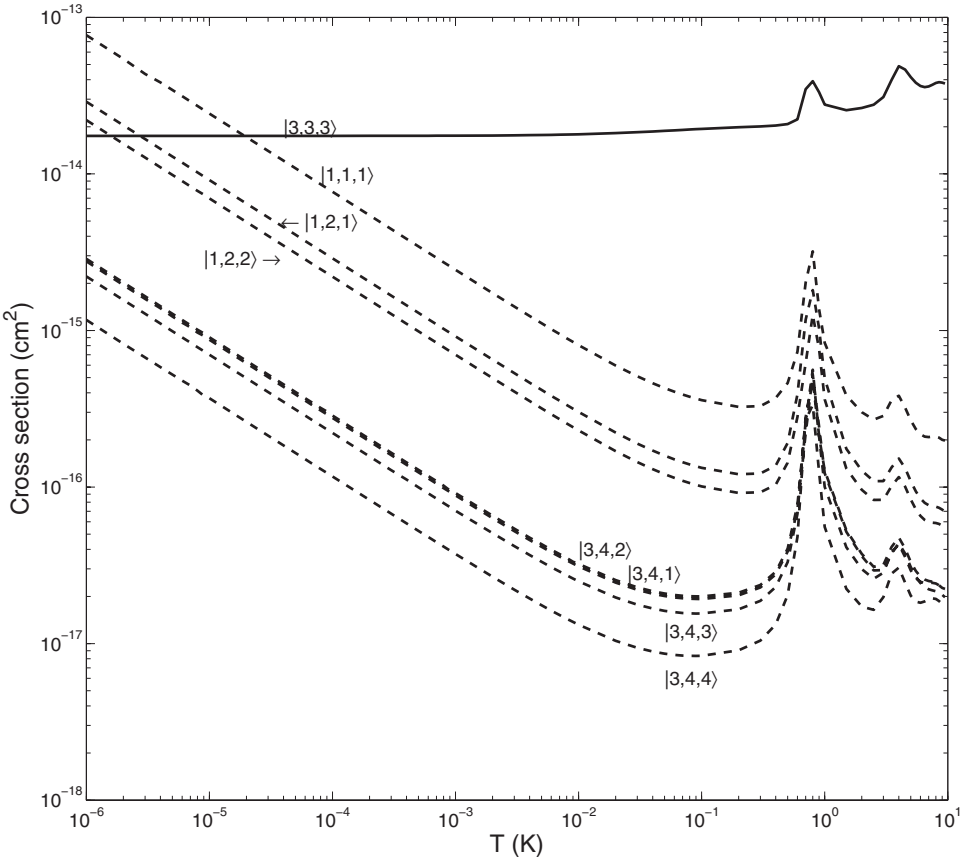

FIG. 6. Cross sections for $|N,J,M_J\rangle \rightarrow |N',J',M_J'\rangle$ with $N=3, J=3, M_J=3$. Cross sections between states not shown in the figure are negligible. Solid line represents elastic scattering.

In addition we have calculated cross sections for rotationally excited molecules in the $N=3$ rotational level. Accurate calculations of the different inelastic cross sections from excited rotational levels are computationally more demanding, as there are many more partial waves that need to be included even at low energies. We show cross sections for molecules initially in the $|3,3,3\rangle$ state (see Fig. 2) in Fig. 6. The elastic cross section is calculated to be of the order 10^{-14} cm^2 and is largely temperature independent away from any resonances, with a slight increase for larger temperatures. The inelastic cross sections are again several orders of magnitudes smaller for temperatures around 1 K; thus rotational cooling as a result of collisions with He is a very limited possibility. The inelastic cross sections are further seen to increase rapidly as the temperature is lowered. Cooling of the translational degree of freedom by elastic collisions may therefore result in more efficient rotational cooling, since the inelastic cross sections for scattering $N=3 \rightarrow N=1$ increases as the temperature is lowered. The behavior of the inelastic cross sections in Fig. 6 can be understood from the Wigner threshold law [32] for inelastic scattering

$$\sigma_{\text{inelastic}} \propto E^{L-1/2}, \tag{27}$$

with $L=0$. A prominent feature in Fig. 6 is the appearance of a resonance at an energy corresponding to $T \simeq 0.8$ K. This represents a shape resonance in the $L=3$ partial wave, confirmed by calculating the elastic partial wave cross sections with only the isotropic part of the potential included: $V(r,\theta)=v_0(r)$.

As previously mentioned, evaporative cooling is needed to reach Bose-Einstein relevant temperatures. However, our calculations cannot be used to predict how efficient O_2 can be evaporatively cooled as this would require knowledge of the O_2-O_2 cross sections. As far as the authors are aware, cross sections for O_2-O_2 have never been calculated due to the complexity of the intramolecular interaction.

We have however studied the buffer cooling process in some detail, based on the cross sections we have calculated. In Table V we report selected calculated cross sections for scattering between the different rotational levels, which are important for the next subsection on buffer-gas cooling.

B. Buffer-gas cooling

Diatomic molecules have noncentral interactions [cf. Eq. (20)] with the buffer gas, thus it is possible to cool both the translational and the rotational degree of freedom. We have simulated the buffer-gas cooling process numerically based on our calculated cross sections $\sigma_{N\rightarrow N'}$. For this purpose we have used the direct simulation Monte Carlo (DSMC) method [33,34] with cross sections from our calculations. The DSMC method is developed from the physics of gas flow and has a close relationship with the Boltzmann equation. The philosophy of the DSMC method is to model a real gas flow with a relative small number of simulated molecules (in general particles). The simulated region in space (three-dimensional) is divided into cells of equal size, with different numbers of molecules in each cell. Initially the molecules are distributed randomly with a random number generator. At

TABLE V. Cross sections $\sigma_{N\to N'}$ for the scattering processes $N\to N'$ at selected temperatures. All values are given in 10^{-17} cm^{-2}.

T(K)	σ_{11}	σ_{33}	σ_{31}	σ_{55}	σ_{53}	σ_{51}	σ_{77}	σ_{75}	σ_{73}	σ_{71}
0.01	1981	1791	134.6	1793	286.1	99.32	1839	112.0	44.27	10.11
0.1	2077	1939	59.25	1930	117.5	42.81	1939	169.1	46.87	8.339
1.0	3830	1448	170.9	2621	571.3	135.2	2622	721.7	45.51	7.101
3.0	3239	1615	52.52	3044	128.5	36.41	3015	175.4	42.14	5.116
5.0	4396	1992	46.17	3990	127.1	35.30	3173	175.1	41.83	3.971
7.0	3745	2611	34.52	3542	90.46	25.70	3417	174.4	41.78	3.611
9.0	3922	2554	31.58	3754	79.14	22.16	3771	151.8	39.40	3.402
11.0	3568	2598	25.75	3467	84.55	19.91	3102	136.3	37.71	3.089
13.0	3211	2689	23.95	3211	75.58	19.18	3615	130.9	35.51	3.012
15.0	3121	2807	23.28	3415	70.84	17.54	3694	125.6	30.57	3.883
17.0	3120	2808	21.25	3268	69.59	15.43	3667	123.6	28.87	3.339
19.0	3063	2762	59.25	3178	66.14	16.99	3594	115.4	22.77	3.735

each time step the molecules are moved $\mathbf{r}_i\to\mathbf{r}_i+\mathbf{v}_i\Delta t$ and may of course in this process change cell. One of the key ideas to the method is the decoupling of translation and collision; the molecules are first moved without any interaction from other molecules or atoms. External forces, e.g., a magnetic field or gravity may be included in the moving step. Interaction with other molecules then proceeds in a collision step *after* the molecules are moved. At each time step some of the molecules are selected to collide and the outcome of these collisions depends on the different cross sections. The energy in each collision is found from the relative velocity and the cross section is estimated from an interpolation in a table of calculated cross sections as a function of energy. Throughout the process each molecule is monitored and information about velocity and rotational levels are updated at every time step. The number of simulated collisions N_{coll} in a cell during a timestep Δt is determined by kinetic theory and is given by

$$N_{\text{coll}}=\frac{N_c(N_c-1)\sigma v_{\max}\Delta t}{2V_c}, \tag{28}$$

where N_c is the number of molecules in a given cell and V_c is the volume of that cell. $v_{\max}$ is an upper limit for the relative velocities. We have used bounce-back (reflecting walls) boundary conditions in the simulations.

For the DSMC method to be reliable the time step Δt must be chosen in such a way that it is smaller than or of the same order as the mean collision time τ. Correspondingly, the cell length should be smaller than the mean free path. The physical parameters used in our simulations yield a mean collision time $\tau=4.2\times10^{-4}$ s and a mean free path $l=1.3\times10^{-2}$ cm.

For our simulation to be as realistic as possible we have assumed a buffer-gas density of 10^{15} cm^{-3}. In the simulations we use 10^6 He atoms and 2000 O_2 molecules. The physical size of the box is determined from the density and number of atoms and molecules. The He atoms are initially at a temperature $T=1.0$ K, while the initial velocity distribution for the O_2 molecules is a delta function with a velocity corresponding to the temperature $T=20$ K, estimated from the relation $E=\frac{3}{2}k_BT$.

Our simulations only account for collisions between the He buffer-gas and the O_2 molecules. Collisions among the O_2 molecules themselves should be rare, whereas collisions between He atoms are rather uninteresting. Initially, the rotational quantum numbers for the O_2 molecules are distributed according to the Boltzmann distribution; see Fig. 7.

After simulation of the buffer gas cooling process for some time we find that the O_2 molecules have been thermalized to a temperature close to the buffer-gas temperature. This is confirmed by plotting the speed distribution together with the Maxwell speed distribution $\mathcal{D}(v)$ for $T=1.0$ K, to observe the excellent agreement. Upon thermalization we also observe the mean speed of the O_2 molecules fluctuate around a mean value.

Figure 8 shows plots of the results of the thermalization process. The (mean) number of collisions per molecule are 8.22, 14.7, 21.5, and 28.7 corresponding to the times t

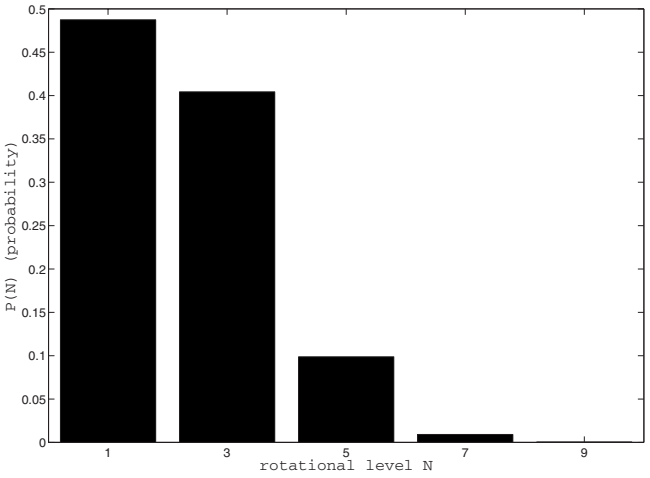

FIG. 7. Probability distribution for different rotational levels N in O_2 at $T=20$ K.

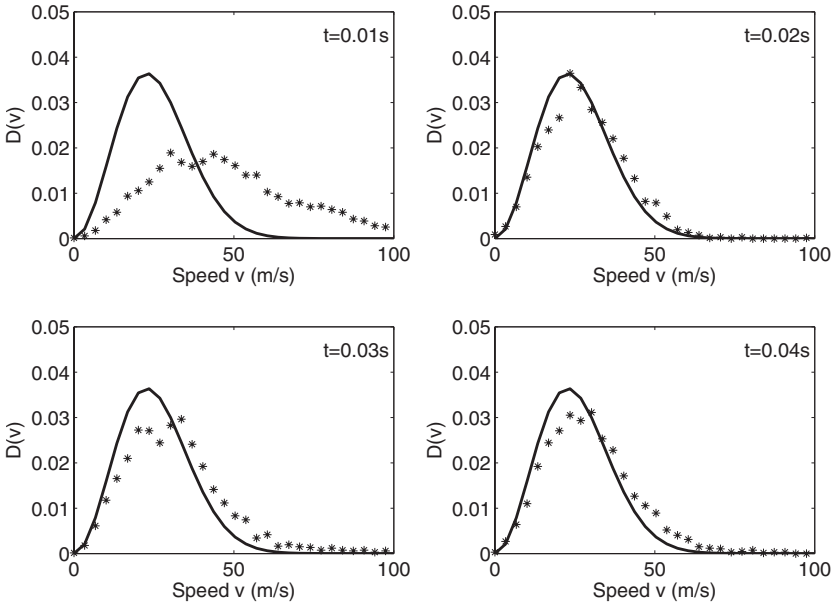

FIG. 8. Speed distribution for O_2 molecules at times $t=0.01$ s, 0.02 s, 0.03 s, and 0.04 s (asterisks), compared to the Maxwell distribution (sold line) plotted at $T=1$ K.

$=0.01$, 0.02, 0.03, and 0.04 s. We conclude that thermalization of the translational degree of freedom for O_2 molecules initially at $T=20$ K with a buffer gas at 1 K requires the O_2 molecules undergo roughly 20 collisions with He.

In our simulations we have also included collisions in which the rotational quantum number N is changed. In a collision with energy E we calculate the probabilities for an allowed transition based on the cross sections. A random number is then generated to determine the outcome of the collision. We do allow for rotational excitations provided that the energy involved is sufficient. It is easily seen from the cross sections that most collisions will be elastic and this should be expected from the calculated PES which is quite isotropic.

Due to the small probabilities for change of the rotational level in a collision, the rotational degree of freedom requires many more collisions to attain a population typical for 1 K (99.9% in $N=1$ according to the Boltzmann distriubution). In Fig. 9 we show the rotational population numbers after times $t=0$, 0.03, 0.1, and 0.5 s. The initial distribution of rotational levels for the O_2 molecules follow the Boltzmann distribution for $T=20$ K (see Fig. 7).

The efficiency of translational and rotational cooling may be compared most easily by the number of collisions required to reach equilibrium. Whereas cooling of the translational freedom is seen to require 15–20 collisions with the buffer gas, the rotational distribution has still not reached an equilibrium distribution after 71 collisions.

V. Na_2-Na SYSTEM

We now turn our attention to Na and study collisions between $^{23}Na_2$ molecules and Na atoms. The Na_2 internuclear separation is kept fixed at $r_e=3.0786$ Å. The Na_2 ground state, $^1\Sigma_g^+$, has neither spin nor angular momenta. Na_2 molecules are usually cooled with other cooling methods apart from buffer-gas cooling. Since the ground state is not magnetically trapable it is also challenging to employ the evaporative cooling technique. Ultracold ground state molecules may instead be a likely result of molecule formation in photoassociation experiments. A two color photoassociation scheme is one example of a cooling method likely to yield ground state Na_2 molecules residing in the lowest attainable vibrational level ($v=0$) [7]. These ultracold ground state molecules will collide with Na atoms not yet photoassociated to a an excited electronic state. As both molecule and atom have temperatures in the μK temperature range, the collisions between them will necessarily be cold. We have computed cross sections for both elastic and inelastic collisions at temperatures ranging from 10^{-9} K to 10^{-2} K, as this should

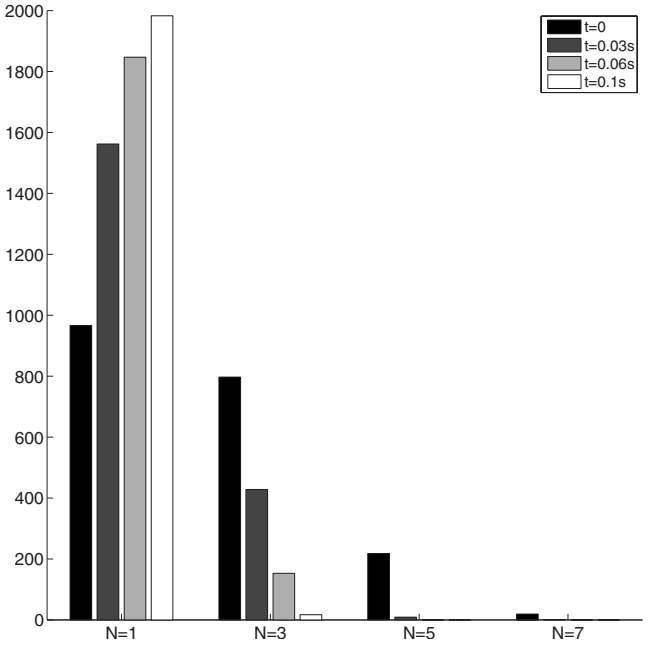

FIG. 9. Rotational distribution for O_2 molecules after $0(t=0)$, $21(t=0.03$ s), $42(t=0.06$ s), and $71(t=0.1$ s) collisions with the He buffer gas.

TABLE VI. Calculated PES for the Na_2-Na interaction. Distances r in a.u. and angles θ in degrees. Energies are given in mE_h. We use the basis set cc-pCTZ [22] for all atoms involved in the calculation.

	θ									
r	0	10	20	30	40	50	60	70	80	90
4.00	2742	2088	1027	425.9	203.8	142.45	30.65	24.80	21.51	18.98
5.00	837.3	656.1	353.9	167.6	85.12	51.24	12.30	5.110	2.968	2.927
6.00	122.1	108.3	78.49	48.89	25.84	10.33	1.314	−3.07	−3.912	−3.460
7.00	33.01	29.66	21.38	11.89	4.068	−1.007	−3.570	−4.389	−4.316	−4.182
8.00	6.008	5.189	2.968	0.4552	−1.723	−3.139	−3.606	−3.535	−3.333	−3.240
9.00	−0.4639	−0.7722	−1.528	−2.318	−2.797	−2.884	−2.709	−2.461	−2.271	−2.202
10.0	−2.406	−2.444	−2.507	−2.494	−2.347	−2.101	−1.836	−1.621	−1.487	−1.443
11.0	−2.223	−2.186	−2.070	−1.879	−1.640	−1.400	−1.194	−1.050	−0.9671	−0.9402
12.0	−1.573	−1.531	−1.415	−1.247	−1.064	−0.8960	−0.7653	−0.6776	−0.6288	−0.6133
13.0	−1.010	−0.9800	−0.8992	−0.7881	−0.6712	−0.5679	−0.4892	−0.4374	−0.4093	−0.4006
14.0	−0.6249	−0.6066	−0.5574	−0.4907	−0.4214	−0.3606	−0.3142	−0.2837	−0.2673	−0.2623
15.0	−0.3843	−0.3737	−0.3453	−0.3067	−0.2665	−0.2312	−0.2039	−0.1857	−0.1759	−0.1728
16.0	−0.2389	−0.2328	−0.2166	−0.1944	−0.1711	−0.1504	−0.1343	−0.1233	−0.1173	−0.1153

be the most relevant temperature range. In the calculations we have included partial waves up to $L=25$.

In Table VI we list the short range PES calculated for $r=4.00$ a.u. to $r=16.0$ a.u.. For $r>16.0$ a.u. we use Eq. (20) with coefficients from Table IV. Small inconsistencies between the long-range PES and the GAMESS PES are resolved by making a smooth transition between the two with a polynomial fit. We do believe that our dispersion coefficients give the most accurate description of the PES at $r=16$ a.u.; thus we have matched the GAMESS PES to the long range PES calculated from dispersion coefficients. Again we have integrated the close coupled Eqs. (3) out to $r=2000$ a.u., starting from $r=4.0$ a.u.

In Fig. 10 we give $v_l(r)$ for the calculated PES. Whereas the O_2-He interaction was given in μE_h, the Na_2-Na interaction is reported in mE_h. This increased interaction energy is

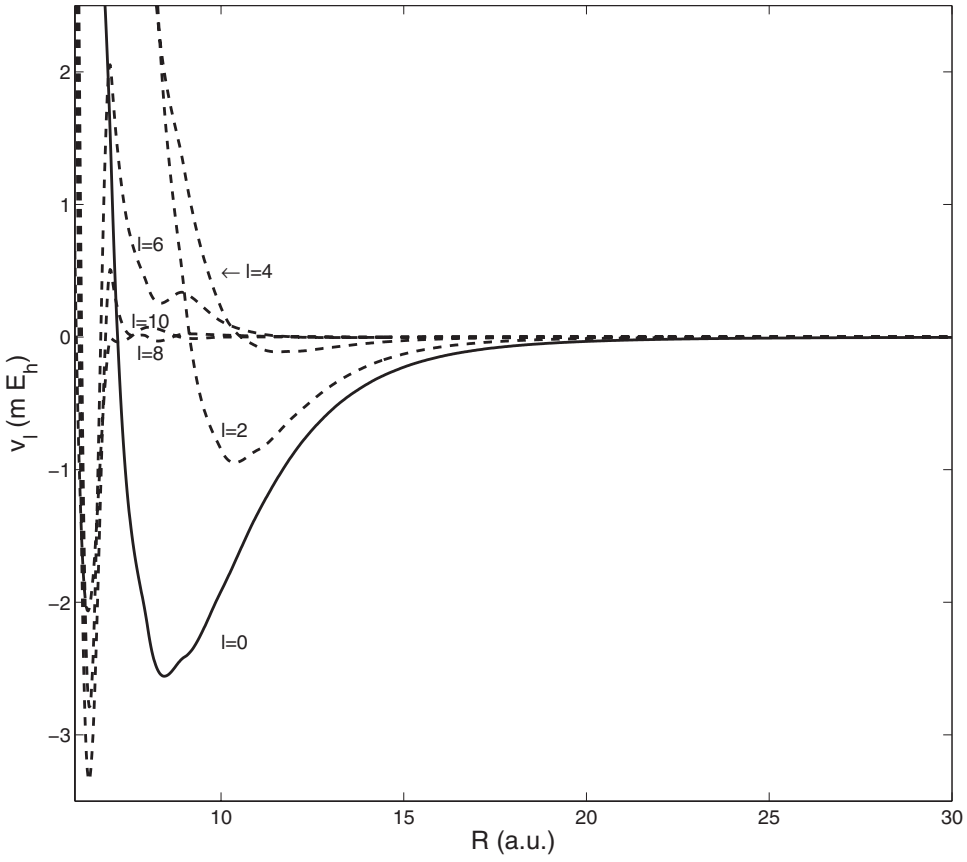

FIG. 10. Different terms $v_l(r)$ [cf. Eq. (6)] for the Na_2-Na interaction.

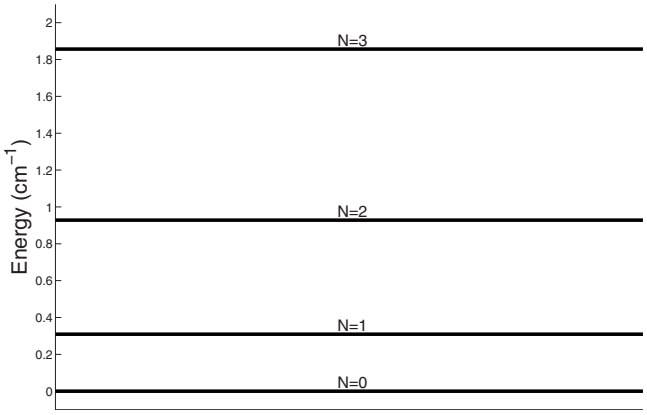

FIG. 11. Rotational energies for the $N=0,1,2,3$ rotational levels in the ground electronic and vibrational state of the Na_2 molecule.

largely due to the valence electron of Na. It is also evident from Fig. 10, that the larger contributions stem from $v_0(r)$, $v_2(r)$, $v_4(r)$, and $v_6(r)$. $v_8(r)$ and $v_{10}(r)$, on the other hand, provide only small corrections. The anisotropic terms in the PES, $v_2(r)$ and $v_4(r)$, are largely responsible for the inelastic scattering between different rotational levels. By comparing Fig. 10 to Fig. 4, the anisotropic terms can be seen to give a larger contribution for the Na_2-Na system than for the O_2-He system. We would thus expect a larger fraction of the total cross section to be inelastic.

All rotational levels are allowed in the $^{23}Na_2$ molecule as the nuclear spin of the Na atom is $I=\frac{3}{2}$. Due to the small rotational constant $B_e=0.154\ 71\ \text{cm}^{-1}$, the rotational levels are packed close together; see Fig. 11. The molecular spin is zero ($\mathbf{S}=0$); thus $\mathbf{N}=\mathbf{J}$ and there is no fine structure in the ground state. The Na atom do however have an open shell, giving a spin $\mathbf{s}=\frac{1}{2}$.

Inelastic scattering processes are only allowed between rotational levels with the same parity. This is a direct consequence of the fact that the Na_2 molecule is homonuclear with only even values of l allowed in the sum in Eq. (6). For the $3j$ symbol involving N and N' in Eq. (9) to be nonzero, $N+N'$ must be an even number. This makes transitions between neighboring rotational levels forbidden, making it impossible for molecules in the $N=1$ rotational level to reach the $N=0$ level through collisions with Na.

The inelastic and elastic cross sections for the four lowest rotational levels are shown in Fig. 12. The cross sections are seen to be several magnitudes larger than for the O_2-He system; this should not be surprising as Na is heavier and extends further in space than both the O and the He atoms. The alkalis are further known to have large cross sections, which is one of the reasons why Bose-Einstein condensates were first obtained with alkalis and not with hydrogen.

The elastic cross sections for the different rotational levels are all of similar size and show many of the same features. Away from any resonances, at mK temperatures, the elastic cross sections are in fact almost identical. This should probably be expected as the rotational constant is small; the energy difference between the rotational levels become more and more negligible as the temperature increases.

The inelastic cross sections do of course increase at low temperatures, as predicted by the Wigner threshold. It is interesting to see that the inelastic cross section, in particular for the $N=3\rightarrow N'=1$ transition, completely dominates over the elastic $N=3\rightarrow N'=3$ transition for temperatures $T<1\ \mu\text{K}$. This indicates that very efficient rotational cooling can be achieved for collisions at these low temperatures. At mK temperatures, the inelastic cross sections are roughly a factor $\frac{1}{40}$ of the elastic ones; thus the possibility of rotational cooling is severely restricted. As we will see, the situation is quite similar for the K_2-K system.

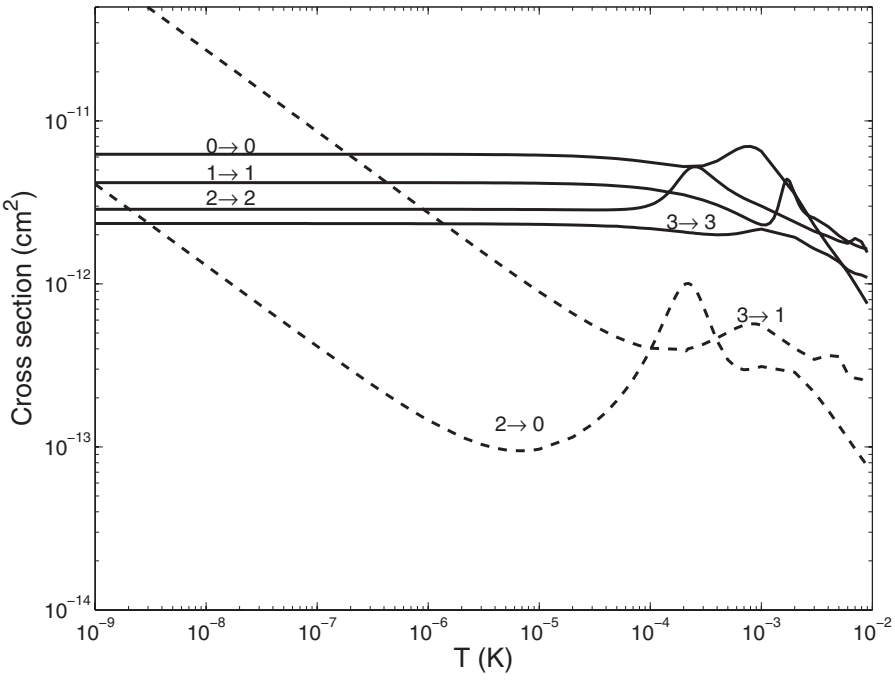

FIG. 12. Elastic and inelastic cross sections for $N=0,1,2,3$ rotational levels in the ground electronic and vibrational state of Na_2. Elastic cross sections are plottes as solid lines.

TABLE VII. Calculated PES for the K_2-K interaction. Distances r in a.u. and angles θ in degrees. Energies are given i mE_h. We have used the triple zeta valence (TZV) [23] basis set augmented with polarization functions of type d.

	θ									
r	0	10	20	30	40	50	60	70	80	90
6.00	2351	1844	966.0	396.8	155.9	70.76	38.78	24.20	21.92	15.65
7.00	437.3	360.6	214.8	108.7	55.42	29.80	15.84	8.148	4.828	10.97
8.00	99.89	87.63	61.94	38.50	21.70	10.40	3.418	−0.2382	−1.475	4.836
9.00	33.29	30.03	22.16	13.22	5.619	0.3255	−2.710	−4.016	−4.158	2.138
10.0	9.678	8.319	4.948	1.048	−2.169	−4.218	−5.188	−5.394	−5.134	1.025
11.0	−1.018	−1.539	−2.809	−4.213	−5.260	−5.794	−5.898	−5.735	−1.947	0.5370
12.0	−5.087	−5.238	−5.586	−5.922	−6.098	−6.085	−5.939	−3.612	0.2887	0.2950
13.0	−6.140	−6.158	−6.187	−6.177	−6.102	−5.969	−3.612	0.1240	0.1548	0.1643
14.0	−6.139	−6.126	−6.084	−6.011	−4.782	−0.07322	0.007790	0.05768	0.08340	0.09118
15.0	−4.783	−4.813	−4.894	−0.2582	−0.1503	−0.06121	−0.007089	0.02748	0.04485	0.05003
16.0	−0.3229	−0.3007	−0.2425	−0.1684	−0.09840	−0.04397	−0.007683	0.01356	0.02403	0.02712
17.0	−0.1912	−0.1778	−0.1431	−0.09899	−0.05763	−0.02587	−0.008761	0.006983	0.01283	0.01540
18.0	−0.1054	−0.09793	−0.07850	−0.05401	−0.03121	−0.03289	−0.01034	0.003745	0.006824	0.007716
19.0	−0.05487	−0.05092	−0.04067	−0.04830	−0.02910	−0.03129	−0.01238	0.001454	0.003613	0.004059
20.0	−0.04821	−0.04551	−0.03771	−0.04445	−0.02832	−0.028760	−0.01436	0.001157	0.001900	0.002113

VI. K_2-K SYSTEM

We now turn our attention to a heavier alkali system, namely the $^{39}K_2$-^{39}K system. As K and Na have many of the chemical properties in common the cross sections may be expected to behave similarly.

Both species have attracted considerable interest in recent years, and translationally ultracold samples of both Na_2 and K_2 molecules may nowdays be produced in the laboratory. As K is heavier than Na it is also more challenging to reliably calculate the interaction between the K_2 molecules and the K atom. Here we report cross sections obtained with the PES calculated with GAMESS at short range and by using the dispersion coefficients (see Sec. III) to reliably model the long range potential. The short range PES obtained is reported in Table VII for $r \in [6.00-20.00$ a.u.].

For all geometries the Hartree-Fock calculations are convergent ($\Delta E < 10^{-6}$ a.u.), although at some geometries the convergence was rather slow. Indeed this was the case for some geometries ($\theta=0-50°$) at $r=15$ a.u. and for a few other spread geometries. The problem is most easily solved by simply performing an additional number of Hartree-Fock iterations or by using a level shift. That is, lifting the diagonal elements of the Fock matrix up (in energy) to uncouple the occupied and unoccupied orbitals. This is a clear indication that the slow convergence stems from electronic states which lie close together, although not exactly degenerate, at least not at the geometries we have investigated. This problem is of course also encountered for atom-atom collisions, although more frequently for atom-molecule collisions as the number of electronic states are much larger.

The internuclear distance for the K_2 molecule was kept at the equilibrium distance of $r_e=3.923$ Å. At $r=20$ a.u. we connect the short-range PES to the long-range PES. Additional consideration is needed to do this as the short-range PES is in fact repulsive for some of the larger values of θ even at $r=20$ a.u., whereas the long-range PES of course is attractive [cf. Eq. (20)]. As a solution we make a smooth transition between the two energy surfaces for $r=20-25$ a.u.. For $r>25$ a.u. we use solely the long range PES. This inconsistency is of course evidence of inaccuracies in one or both of the calculated surfaces. As we do believe the long-range PES is the most reliable of the two surfaces, we have modified the short range PES to match the long range PES at $r=25$ a.u.

The K_2-K PES is expanded in Legendre polynomials [cf. Eq. (6)]. As the PES is quite anisotropic we have needed to include Legendre polynomials for $l \in [0,40]$ to ensure a representation of the PES with at least two leading digits of accuracy for all geometries. Figure 13 gives the first functions v_l for $l=0-10$ and should be compared to Fig. 10. The strong anisotropy in the PES (Table VII) affects the behavior of the plotted terms $v_l(r)$; all terms yield significant contributions.

K_2 molecules have a ground state rotational constant $B_e=0.056\ 22\ \mathrm{cm}^{-1}$ with a rotational structure as shown in Fig. 14. We give the cross sections for the lowest rotational levels, of relevance for cold and ultracold collisions.

From Fig. 15 we may note the following. (1) The elastic cross section is a factor 10 larger for elastic collisions $N=1 \rightarrow N'=1$ than for any other elastic collision process at ultralow energies. The $N=1 \rightarrow N'=1$ elastic cross section is several orders of magnitude larger than the $N=0 \rightarrow N'=0$ elastic cross section. (2) For temperatures in the mK range, away from any resonances, the different elastic cross sections are of equal magnitude, whereas inelastic collisions are suppressed. (3) The Wigner threshold law is obeyed at ultralow energies.

Cross sections are known to be very sensitive for changes in the scattering potential, in particular at low energies. To

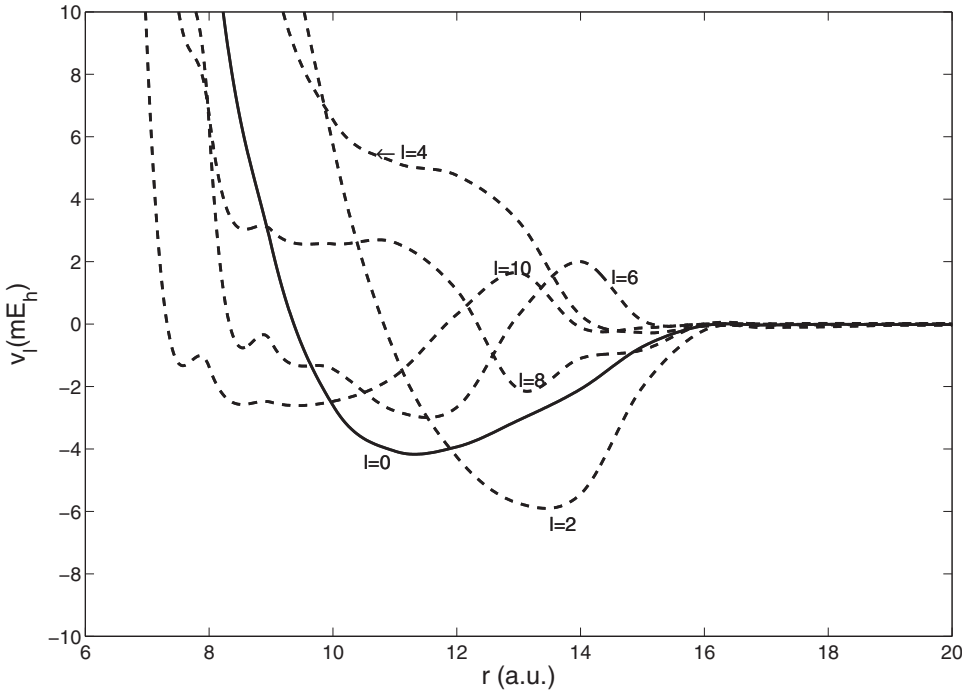

FIG. 13. Different terms $v_l(r)$ for $l=0,2,4,6,8,10$ [Eq. (6)] for the K_2-K interaction.

see just how sensitive the scattering cross sections are for changes in the long range potential, we increased the dispersion coefficients (Table III) for the K_2-K system by 10% and recalculated the cross sections for $N=0$. The elastic cross section at $T=1$ nK increased by about 1000%, whereas the elastic cross section at $T=1$ mK decreased by 30%. This certainly demonstrates how sensitive the scattering cross sections are for changes in the long range PES at ultracold temperatures and shows the importance of a reliable long range PES. Similar demonstrations can be made for the O_2-He and Na_2-Na systems, although the effect is not as dramatic.

VII. CONCLUSIONS

We have calculated the PES for three different systems, O_2-He, Na_2-Na, and K_2-K, with special emphasis on the long range interaction, which as we have seen is of utmost importance for reliable scattering calculations. The van der Waals coefficients defining the long range PES have been calculated from the polarizabilities and are expected to be of high accuracy. With the obtained potential energy surfaces we have solved the coupled equations to obtain elastic and inelastic cross sections for transitions between different rotational levels and Zeeman levels (for O_2-He).

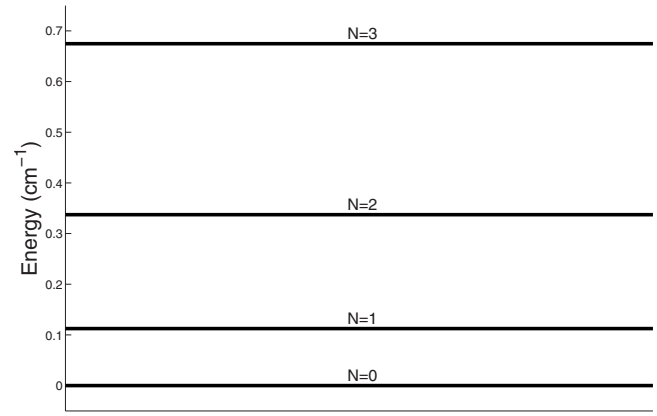

FIG. 14. Rotational energies for the $N=0,1,2,3$ rotational levels in the ground electronic and vibrational state of the K_2 molecule.

All reported cross sections have been calculated with a large number of partial waves included, to ensure satisfactory convergence. Most calculations have involved partial waves with $L>20$.

For buffer-gas cooling of O_2 molecules with He atoms we predict macroscopic properties such as speed distributions, temperature, and number of collisions needed to thermalize the O_2 molecules based on the calculated cross sections. Magnetic trapping of O_2 molecules in the ground electronic and rovibrational state is predicted to be feasible and trap loss from collisions with He is expected to be limited. Detailed predictions can however not be given as all cross sections are calculated in zero magnetic field.

For all systems the Wigner threshold law is obeyed at low energies and we have found the inelastic cross sections to be larger than the corresponding elastic ones when the energy is sufficiently low, yielding efficient rotational cooling at ultracold temperatures. For O_2-He, the inelastic transitions $N=3 \rightarrow 1$ dominates over the corresponding elastic transition for $T<10^{-5}$ K, whereas the temperatures are respectively $T<10^{-6}$ K and $T<10^{-8}$ K for the same phenomena to occur in the Na_2-Na and K_2-K systems.

Further, the elastic cross sections for the K_2 molecule are different by several orders of magnitude depending on the rotational level, favoring the $N=1$ level. This is in contrast to the Na_2-Na system where the elastic cross section for different rotational levels is of a similar magnitude for all calculated temperatures. Inelastic rotational scattering is for all systems seen to be suppressed for temperatures in the mK range.

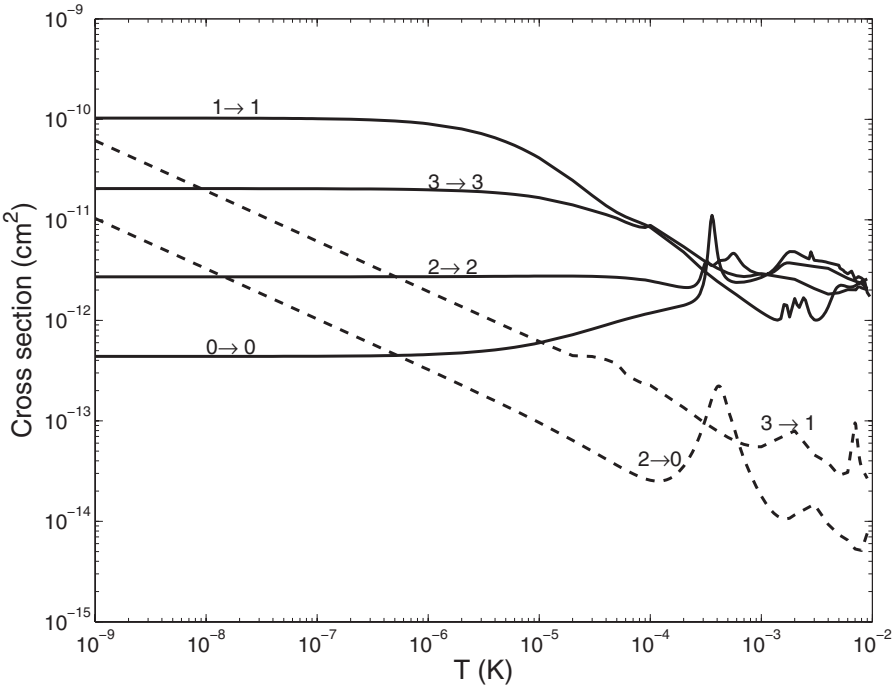

FIG. 15. Elastic and inelastic cross sections for $N=0,1,2,3$ rotational levels in the ground electronic and vibrational state of K_2.

For future studies it would be interesting to include magnetic fields and calculate their influence on the cross sections. With relevance to photoassociation experiments it would furthermore be of considerable interest to include excited vibrational levels in a similar study.

ACKNOWLEDGMENT

Both authors want to acknowledge Inge Røeggen at the University of Tromsø (UiT) for his useful input regarding PES calculations.

[1] J. T. Bahns, W. C. Stwalley, and P. L. Gould, J. Chem. Phys. **104**, 9689 (1996).
[2] M. Greiner, C. A. Regal, and D. S. Jin, Nature (London) **426**, 537 (2003).
[3] S. Jochim, M. Bartenstein, A. Altmeyer, G. Hendl, S. Riedl, C. Chin, J. H. Denschlag, and R. Grimm, Science **302**, 2101 (2003).
[4] M. W. Zwierlein, C. A. Stan, C. H. Schunck, S. M. F. Raupach, S. Gupta, Z. Hadzibabic, and W. Ketterle, Phys. Rev. Lett. **91**, 250401 (2003).
[5] H. Feshbach, Ann. Phys. (N.Y.) **5**, 357 (1958).
[6] H. R. Thorsheim, J. Weiner, and P. S. Julienne, Phys. Rev. Lett. **58**, 2420 (1987).
[7] Y. B. Band and P. S. Julienne, Phys. Rev. A **51**, R4317 (1995).
[8] W. C. Stwalley, Prog. Quantum Electron. **8**, 203 (1984).
[9] J. M. Doyle, B. Friedrich, J. Kim, and D. Patterson, Phys. Rev. A **52**, R2515 (1995).
[10] J. L. Bohn, Phys. Rev. A **62**, 032701 (2000).
[11] P. Soldan, M. T. Cvitas, J. M. Hutson, P. Honvault, and J.-M. Launay, Phys. Rev. Lett. **89**, 153201 (2002).
[12] M. T. Cvitas, P. Soldan, J. M. Hutson, P. Honvault, and J.-M. Launay, Phys. Rev. Lett. **94**, 033201 (2005).
[13] G. Quemener, P. Honvault, J. M. Launay, P. Soldán, D. E. Potter, and J. M. Hutson, Phys. Rev. A **71**, 032722 (2005).
[14] A. M. Arthurs and A. Dalgarno, Proc. R. Soc. London, Ser. A **256**, 540 (1960).
[15] M. S. Child, *Molecular Collision Theory* (Academic Press Inc., London, 1974).
[16] D. M. Brink and G. R. Satchler, *Angular Momentum*, 3rd ed. (Clarendon Press, Oxford, 1993).
[17] B. R. Johnson, J. Comput. Phys. **13**, 445 (1973).
[18] M. W. Schmidt *et al.*, J. Comput. Chem. **14**, 1347 (1993).
[19] J. H. van Lenthe and F. B. van Duijneveldt, J. Chem. Phys. **81**, 3168 (1984).
[20] C. M. Aikens, S. P. Webb, R. L. Bell, G. D. Fletcher, M. Schmidt, and M. S. Gordon, Theor. Chem. Acc. **110**, 233 (2003).
[21] T. H. Dunning, J. Chem. Phys. **90**, 1007 (1989).
[22] D. E. Woon and T. H. Dunning, Jr., J. Chem. Phys. **103**, 4572 (1995).
[23] D. E. Woon and T. H. Dunning, Jr., J. Chem. Phys. **100**, 2975 (1994).
[24] A. D. McLean and G. S. Chandler, J. Chem. Phys. **72**, 5639 (1980).
[25] G. C. M. Gutowski, F. B. van Duijneveldt, G. Chałasiński and L. Piela, Mol. Phys. **61**, 233 (1986).
[26] S. F. Boys and F. Bernardi, Mol. Phys. **19**, 553 (1970).
[27] L. Veseth, Phys. Rev. A **44**, 358 (1991).
[28] D. M. Bishop and J. Pipin, Int. J. Quantum Chem. **45**, 349 (1993).
[29] U. Hohm, Chem. Phys. **179**, 533 (1994).

[30] L. Veseth and A. Lofthus, Mol. Phys. **27**, 511 (1974).
[31] B. H. Bransden and C. J. Joachain, *Physics of Atoms and Molecules* (Longman Scientific & Technical, New York, 1983).
[32] E. P. Wigner, Phys. Rev. **73**, 1002 (1948).
[33] G. A. Bird, *Molecular Gas Dynamics* (Clarendon Press, Oxford, 1976).
[34] K. Koura, Phys. Fluids **29**, 3509 (1986).